iScience

CellPress
OPEN ACCESS

Article

Wide-range and selective detection of SARS-CoV-2 DNA via surface modification of electrolyte-gated IGZO thin-film transistors

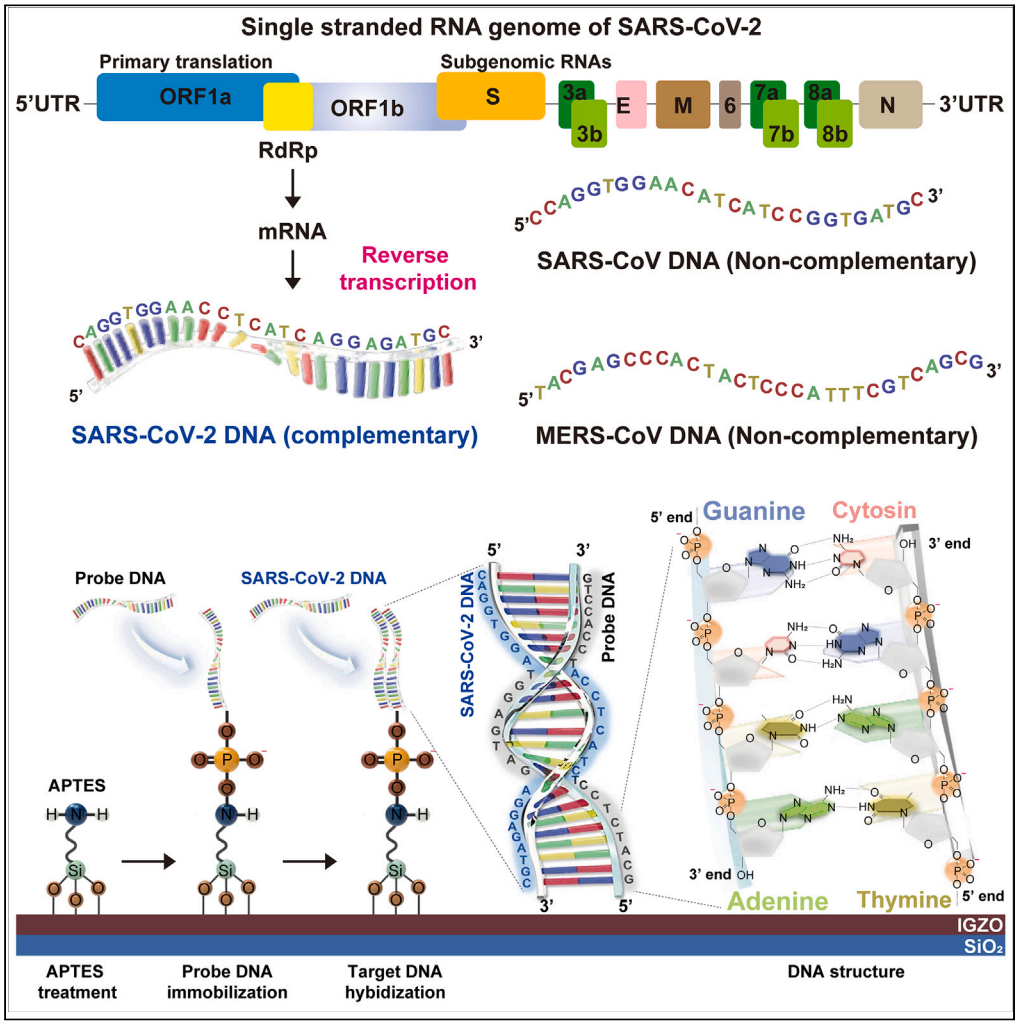

Chuljin Hwang, Seokhyeon Baek, Yoonseok Song, Won-June Lee, Sungjun Park

sj0223park@ajou.ac.kr

Highlights

IGZO-EGTFTs for highly sensitive and wide-range detection of SARS-CoV-2 DNA

IGZO active layer chemically modified for selective hybridization via probe DNA

Physicochemical analytical techniques employed to confirm surface modification

Fully recyclable IGZO biosensor demonstrated with cost-effective fabrication

Hwang et al., iScience 27, 109061
March 15, 2024 © 2024
https://doi.org/10.1016/j.isci.2024.109061

iScience

CellPress
OPEN ACCESS

Article

Wide-range and selective detection of SARS-CoV-2 DNA via surface modification of electrolyte-gated IGZO thin-film transistors

Chuljin Hwang,[1] Seokhyeon Baek,[2] Yoonseok Song,[2] Won-June Lee,[3] and Sungjun Park[1,2,4,*]

SUMMARY

The 2019 coronavirus pandemic resulted in a massive global healthcare crisis, highlighting the necessity to develop effective and reproducible platforms capable of rapidly and accurately detecting SARS-CoV-2. In this study, we developed an electrolyte-gated indium-gallium-zinc-oxide (IGZO) thin-film transistor with sequential surface modification to realize the low limit of detection (LoD <50 fM) and a wide detection range from 50 fM to 5 μM with good linearity (R^2 = 0.9965), and recyclability. The surface chemical modification was achieved to anchor the single strand of SARS-CoV-2 DNA via selective hybridization. Moreover, the minute electrical signal change following the chemical modification was investigated by in-depth physicochemical analytical techniques. Finally, we demonstrate fully recyclable biosensors based on oxygen plasma treatment. Owing to its cost-effective fabrication, rapid detection at the single-molecule level, and low detection limit, the proposed biosensor can be used as a point-of-care platform to perform timely and effective SARS-CoV-2 detection.

INTRODUCTION

Severe acute respiratory syndrome coronavirus 2 (SARS-CoV-2), which was first reported in the city of Wuhan, China, has severely impacted global healthcare standards and economies owing to its rapid aerosol transmission,[1] high potential for genomic recombination,[2] and human-to-human transmission.[3] As of February 17, 2023, more than 756 million cumulative cases, including six million cumulative deaths, have been reported worldwide by the World Health Organization (WHO) (https://covid19.who.int). Although vaccines against SARS-CoV-2 have been available to the public since late 2020 and early 2021, their cost, effectiveness, need for multiple administrations, and potential for adverse events have made them controversial.[4,5] In this regard, the crucial aspects to be considered in the pandemic management include the prevention of transmission and early detection and isolation of asymptomatic patients with SARS-CoV-2 at an early stage.[6] Additionally, large-scale diagnostic testing platforms are required to develop robust surveillance systems via accurate and timely diagnosis.

The WHO recommends the polymerase chain reaction (PCR) assay based on the hybridization of labeled target DNA to a complementary DNA as the global gold standard for diagnosing SARS-CoV-2 infection in clinical practice. This is considered a highly effective method owing to its high specificity, estimated to be close to 100%.[7] However, despite this advantage of the PCR assay, the lack of resources such as specific and dedicated laboratories, skilled technicians, specialized facilities, and sophisticated equipment remains a major challenge. Moreover, the need to resolve several limitations, such as sample collection, transportation, storage, and processing time for sample amplification to achieve sufficient sensitivity and selectivity, has encouraged the development of a rapid and simple platform for onsite and point-of-care (POC) diagnostics to perform massive screening of SARS-CoV-2.

To overcome the limitations of the PCR assay, research on rapid test kits for performing immunoassays to diagnose SARS-CoV-2 infection has been introduced.[8–11] Immunoassays for SARS-CoV-2 diagnosis can detect antibodies against several envelope proteins, including the spike protein, nucleocapsid protein, and receptor-binding domain.[12,13] Although numerous immunoassay-based test kits have been developed, some of them exhibit unsatisfactory diagnostic performance with cross-reactions from other biomolecular constituents and false-positive or false-negative results that mislead patients.[14,15] Furthermore, the reported test results of SARS-CoV-2 may not be reliable because of factors such as limited testing capacity, incomplete reporting, and differences in testing strategies and protocols for individuals. Most test kits employ disposable test pads, limiting the availability of reusable test kits. Therefore, developing DNA detection technologies with high sensitivity, specificity, and recyclability is necessary to facilitate cost-effective and accurate diagnoses via a POC testing platform.

Electrolyte-gated thin-film transistors (EGTFTs) using metal oxide (MOx)-based semiconductors have shown promising potential as a viable alternative to traditional POC testing platforms for SARS-CoV-2 diagnosis owing to their properties such as large-area processes,[16]

[1]Department of Electrical and Computer Engineering, Ajou University, Suwon, Gyeonggi-do 16499, Republic of Korea
[2]Department of Intelligence Semiconductor Engineering, Ajou University, Suwon, Gyeonggi-do 16499, Republic of Korea
[3]Department of Chemistry, Purdue University, West Lafayette, IN 47907, USA
[4]Lead contact
*Correspondence: sj0223park@ajou.ac.kr
https://doi.org/10.1016/j.isci.2024.109061

high mobility,[17] large current on/off ratio,[18] and rapid transient response.[19] Moreover, their large electrical double-layer (EDL) capacitance formed at the boundary between a sensing surface and an electrolyte solution facilitates a low operating voltage,[20] high sensitivity[21] with reliability,[22] and rapid transient response in biological solutions,[23] render it highly amenable to biomolecular sensors.[24] For instance, in a previous study, we developed a biosensor capable of detecting iodide ions in artificial urine with quantitative detection (from 1 to 10^4 μM).[25] Due to the high EDL between the electrolyte and IGZO surface and the rapid redox reaction of iodide ions, the biosensor enabled low voltage operation (<0.5 V) and rapid transient response (<1.0 s), respectively.

However, detecting extremely low concentrations, particularly those below picomolar levels, while maintaining a wide detection range with linear responses, remains a challenge when translating biological reactions into electrical signals. In addition, studies reported some success in the detection of SARS-CoV-2, but quantitative detection for qualitative diagnosis remains a challenge. This is primarily owing to the difficulty in controlling the nanoscale biofunctionalization at solid-liquid interface. Furthermore, it is important to consider the surface properties of the IGZO surface when detecting low concentrations of the target DNA in the presence of other biomolecules such as ions, proteins, carbohydrates, lipids, and nucleic acids. This consideration is also essential for achieving high selectivity in the specific sequence of DNA. To significantly improve the sensitivity and reliability of the biosensor, it is necessary to have an in-depth study on both the electrical and the chemical response of the functionalized IGZO surface.

In this study, we report an innovative SARS-CoV-2 DNA biosensor, demonstrating exceptional sensitivity and a broad detection spectrum through step-by-step comprehensive investigation into both the electrical and chemical responses of the functionalized IGZO surface. The biosensor operates at a low voltage of less than 1V, which is lower than the electrolysis voltage based on indium-gallium-zinc-oxide electrolyte-gated thin-film-transistors (IGZO-EGTFTs). Through a meticulously performed, sequential process of molecular modification on the surface of the indium-gallium-zinc-oxide (IGZO), we have enhanced the anchoring capacity for probe DNA. This probe DNA has been designed specifically to recognize and bind with SARS-CoV-2 DNA, facilitating an efficient hybridization between the probe and the target DNA. Furthermore, the systematic molecular alteration of the IGZO surface can achieve an impressively low detection limit of 50 fM, while also offering a broad detection range from 50 fM to 5 μM. Considering the low costs, the low detection limit, broad detection range with good linearity (R^2 = 0.9965), and excellent reusability, this biosensor can be employed as a point-of-care tool, enabling timely and effective detection of SARS-CoV-2.

RESULTS AND DISCUSSION

Electrical characteristics of IGZO-EGTFTs

Figures 1A and 1B show an illustration and optical microscope image of the IGZO-EGTFTs comprising an IGZO sensing layer with source and drain (S/D) electrodes. Since the operating environment must be considered for IGZO-EGTFTs in an aqueous solution, the device structure adopted a top-gate bottom-contact structure. Therefore, the solution-processed IGZO sensing layer was deposited on S/D electrodes as the active channel in the EGTFTs. Moreover, it offered the advantage of the IGZO channel acting as a passivation layer for preventing the leakage current generated by the contact between the S/D electrodes via the electrolyte during the operation. Further details on the fabrication process are presented in Figure S1. The gate electrode (Ag/AgCl reference electrode (RE)) was immersed into the polydimethylsiloxane (PDMS) well, and the controlled amount of electrolytes with a fixed analyte concentration was tested. The operation of the IGZO-EGTFTs, which functioned as n-type transistors, depended on the formation of an EDL with a very high capacitance at the interface between IGZO and the electrolyte. To form proton-electron pairs, mobile ions were rearranged by applying a positive voltage. Similar to the results of our previous study, an EDL capacitance of 6.2 μF/cm^2 was achieved at 10 kHz, which is 1,000 times higher than the capacitance of the thermally oxidized 300-nm-thick SiO_2 substrate (11.6 nF/cm^2).[26] The high capacitance of the EDL facilitated the IGZO-EGTFT operation at a low voltage.

Figures 1C and 1D show the electrical characteristics tested via the transfer and output curve measurements (i.e., sweeping V_{GS} and V_{DS} in the ranges of −0.5–1 V and 0–1 V, respectively) in a PBS solution when the channel width-to-length ratio was 200/10 μm. For the electrical performance of the IGZO-EGTFTs, various parameters, such as the subthreshold swing (S.S.) (Figure 1E), transconductance (g_m) (Figure 1F), and threshold voltage (V_{TH}) (Figure 1G) were evaluated under PBS solutions. An S.S. ($\partial V_{GS}/\partial \log I_{DS}$) of 66.085 mV/dec was obtained near the theoretical limit in the metal-oxide-semiconductor field-effect transistor (MOSFET).[27] Such a low S.S. guaranteed the excellent switching performance of the fabricated device under an ultra-low operational voltage (<1 V). In addition, g_m, which is another vital parameter defined as $\Delta I_{DS}/\Delta V_{GS}$, indicated that the degree of voltage amplification possible using the IGZO-EGTFT was in accordance with the gate signal (Ag/AgCl RE). This implied a high switching speed and sensitivity when functioning as a biosensor. The calculated average max g_m of 1.005 mS in the switching-off situation is consistent with the result obtained in our previous work.[25] A small hysteresis was observed at a width-to-length ratio of 20, as shown in Figure S2. Furthermore, the V_{TH} shift is an important parameter in IGZO-EGTFTs that can potentially influence the functionality of the biosensor. The calculated average V_{TH} was obtained as 0.126 V using the conventional linear extrapolation method for the drain current in the linear region. The presented statistical data demonstrate excellent uniformity of IGZO-EGTFTs fabricated by spin coating method operating at a low voltage under physiological environments (Figure S3).

Operational mechanism of SARS-CoV-2 biosensor

Figure 2A depicts a schematic of the domain organization of the SARS-CoV-2 RNA and the hybridization process between the probe and SARS-CoV-2 DNA. In this study, a major sequence from the RNA-dependent RNA polymerase genes specific for SARS-CoV-2 was selected as the probe DNA (5′-Phosphate-GCA TCT CCT GAT GAG GTT CCA CCT G-3′). To perform the experiments on the DNA biosensor, the

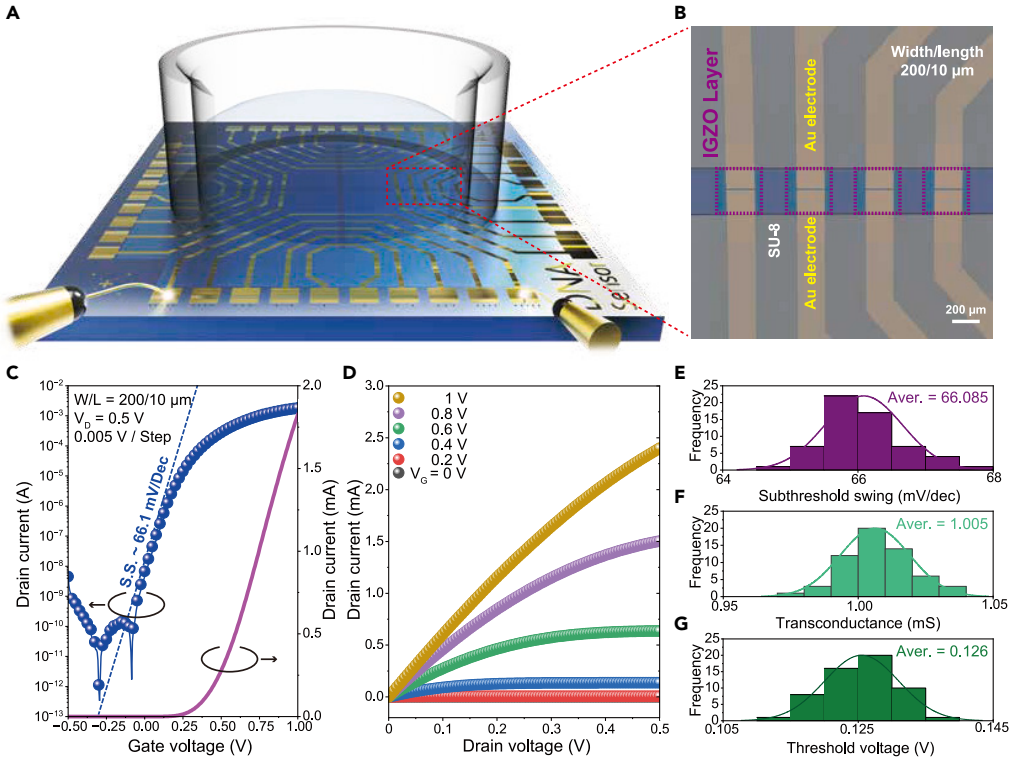

Figure 1. Electrical characteristics of indium-gallium-zinc-oxide (IGZO)-based electrolyte-gated thin-film transistors (EGTFTs) using PBS solution

(A) Schematic showing the device structures for EGTFT with the IGZO sensing layer. IGZO-EGTFT fabricated on the silicon substrate (total 20 devices) with solution-processed IGZO channel measuring 15 × 15 mm^2.

(B) Top view of the optical microscopy image of the top-gate bottom-contact EGTFT for DNA biosensor. The dimensions of the IGZO channel are 200 × 10 μm^2. Scale bar in the image is 200 μm.

(C) Transfer characteristics (I_{DS} vs. V_{GS}) measured at V_{DS} = 0.5 V (V_{GS} = −0.5–1 V), and (D) output characteristics (I_{DS} vs. V_{DS}) of the IGZO-EGTFT device (at V_{GS} = 0, 0.2, 0.4, 0.6, 0.8, and 1 V). Histograms of (E) subthreshold swing, (F) transconductance, and (G) threshold voltage with width/length = 200 μm/10 μm.

genes for SARS-CoV-2 (complementary DNA), SARS-CoV[28] (non-complementary DNA), and MERS-CoV[29] (non-complementary DNA) DNA were synthesized for this study, as shown in Table S1.

Figure 2B illustrates the sensing mechanism involved for SARS-CoV-2 DNA detection via surface modification with 3-aminopropyltriethoxysilane (APTES) and probe DNA on the IGZO active layer. Surface modification with APTES is a commonly employed technique to functionalize the surfaces of various materials, including glass,[30] silicon,[31] and metal oxides.[32] APTES is a silane coupling agent that contains an amino group with a triethoxysilyl group, which facilitates its binding to the surface of the IGZO sensing layer and aids in the formation of a stable covalent bond for the immobilization of DNA,[33] antibodies,[34] and enzymes.[35] Common strategies to immobilize the probe DNA on an IGZO surface include covalent immobilization between the probe DNA and APTES, formation of the probe DNA on gold surfaces,[36] absorption via non-covalent interactions,[37] layer-by-layer polyelectrolyte assembly,[38] and modification of the probe DNA on chemically functionalized surfaces.[39] Among them, the most widely used method to achieve covalent immobilization of the probe DNA is chemisorption onto chemically functionalized surfaces, which exploits the strong affinity interaction between APTES and the phosphate group of the probe DNA, forming a covalent bond. This results in a stable and long-lasting attachment.[40] Unlike the N-doping effect on graphene-based transistors,[41,42] our IGZO-EGTFTs employ EDL as a gate-insulating medium, with highly dense surface charges aligning with oppositely charged ions at the electrolyte-IGZO interface. When IGZO-EGTFTs capture SARS-CoV-2 DNA using immobilized probe DNA at the optimal condition, the phosphate groups on the DNA backbone induced the accumulation of negatively charged carriers on the IGZO channel. Consequently, a significant shift of the transfer curve is obtained owing to the negatively charged surfaces, which results in an increase in V_{TH}.

Surface analysis of reactive site of SARS-CoV-2 biosensor

The detection of DNA in biological solutions, such as saliva, serum, and PBS, is challenging owing to low concentrations of the target (SARS-CoV-2) DNA. To improve the sensitivity of DNA detection, the active site of the crosslinker should be chemically functionalized. Moreover, when analyzing complex biological solutions, there is a risk of non-specific detection of other biomolecules and interference from other biomolecular processes, which may lead to false-positive results. Therefore, a sophisticated biofunctionalization strategy is required to

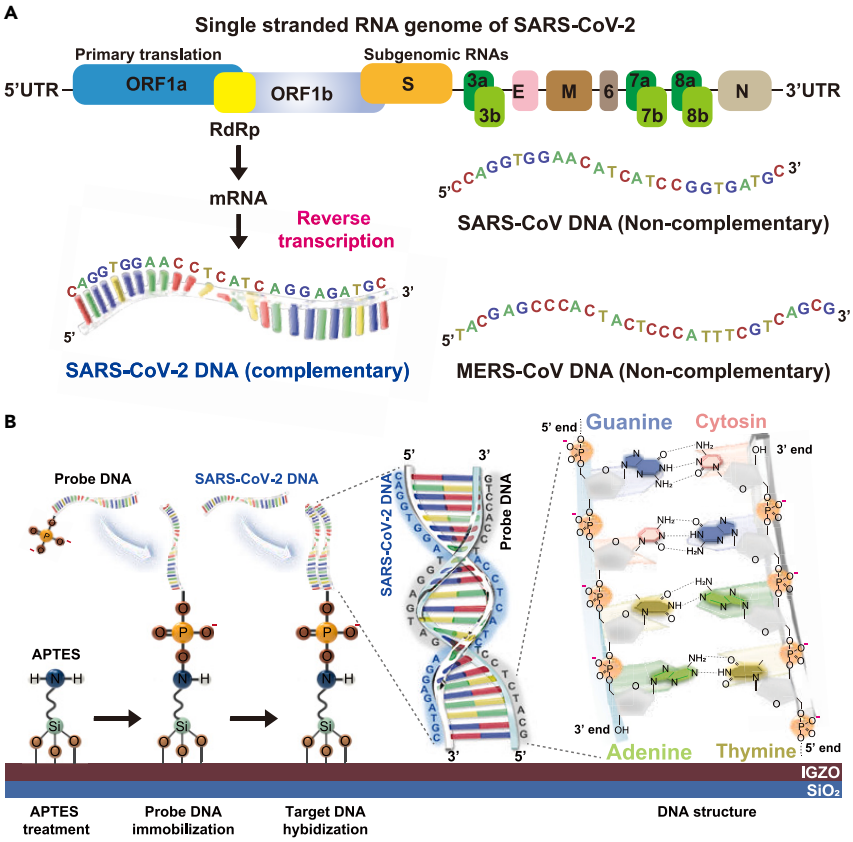

Figure 2. Design of DNA sequence and biosensor based on IGZO-EGTFTs

(A) Schematic for domain organization of severe acute respiratory syndrome coronavirus 2 (SARS-CoV-2) RNA genome. The SARS-CoV-2 DNA (complementary DNA) was composed of reverse transcription sequences from RNA-dependent RNA polymerase (RdRp) of SARS-CoV-2 RNA. SARS-CoV and MERS-CoV DNA (non-complementary DNA) were used to confirm the selectivity of IGZO-EGTFTs.

(B) Functionalization of the IGZO surface for detecting SARS-CoV-2 DNA involves a sequence of steps: treatment with APTES, immobilization of probe DNA, and hybridization with SARS-CoV-2 DNA.

capture the target DNA and ensure precise detection. In Figure 3, the step-by-step analyzation and verification are shown for surface modification of IGZO. Figure 3A and Table S2 show the water contact angle (WCA) and the surface energy, which is calculated via the Girifalco-Good-Fowkes-Young method,[43] with different surface modifications such as APTES treatment, probe DNA immobilization, and complementary DNA hybridization. To ensure accuracy, the WCA was measured as the average of the measurements from three repetitive trials. The initial WCA and surface energy of pristine IGZO were 51.6° and 59.6 mN/m, respectively. Following the oxygen plasma and APTES deposition processes, the WCA increased from 0.8° to 68.1° and the surface energy dramatically decreased to 42.2 mN/m; this can be attributed to a compact formation of self-assembled monolayer (SAM) on the surface of IGZO and the silanol groups of APTES.[44] This trend was verified by depositing 1%, 5%, 10%, and 15% APTES. According to increasing APTES concentration, WCA increases from 0.8° to 39.1°, 64.8°, 68.1°, and 75.6°, and the surface energy decreases from 70.6 to 46.3, 42.2, and 35.2 mN/m, respectively, as shown in Figure S4 and Table S3. The result indicates that the surface of IGZO became more hydrophobic following the amino-terminated surface modification. The process of DNA immobilization was employed on an IGZO surface with APTES treatment of 10%. This particular concentration was chosen as it demonstrated reliable and repeatable results in experimental settings, thereby ensuring the success of the DNA attachment procedure. Following the immobilization of the probe DNA onto APTES, the increase in WCA from 68.1° to 79.1° and the decrease in surface energy from 42.2 to 38.8 mN/m can be attributed to the hydrophobic carbon of the probe DNA, indicating a successful covalent binding between APTES and the probe DNA.[45] After hybridization between probe DNA and SARS-CoV-2, the WCA and surface energy reach 73.1° and 37.3 mN/m, indicating the IGZO surface shows more hydrophilic behavior due to the hydrophobic carbon of the hybridized SARS-CoV-2.

To monitor molecular compounds resulting from chemical reactions and the DNA assembly at the IGZO surface, ATR-FT-IR analysis with the scan range from 1,500 to 4,000 cm^{-1} was conducted as shown in Figure 3B. After the APTES were deposited, 1,568 cm^{-1} related peaks were assigned to the NH_2 deformation nodes of the amine groups,[46] and the two peaks at 2,847 and 2,953 cm^{-1} were attributed to C–H stretching.[47] These three peaks indicate that APTES has been successfully deposited on the IGZO surface. As shown in Figure S5, the distinctive peaks associated with silanization were observed across all concentrations of APTES (from 1% to 15%), with the intensity of the peaks

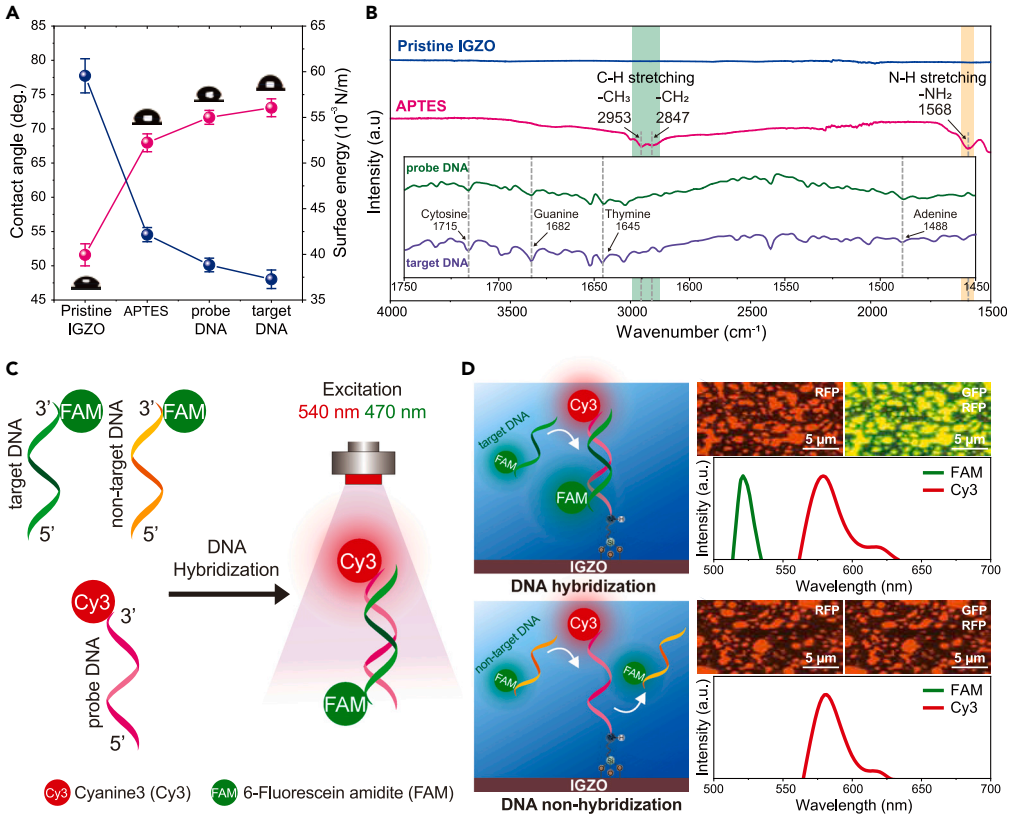

Figure 3. Surface analysis of IGZO-EGTFT biosensor for detecting SARS-CoV-2

(A) Water contact angle (WCA) measurement and calculated surface energy to confirm hydrophobic characteristics on the IGZO surface with pristine IGZO, APTES, probe DNA, and SARS-CoV-2 DNA. The insets correspond to the water droplet shape and angles based on the specific surface condition.

(B) Fourier transform infrared spectra (FT-IR) of the IGZO surface with IGZO, APTES, probe DNA, and SARS-CoV-2 DNA. The spectra were obtained without corrections from 64 transmission scans with 4 cm^{-1} resolution and analyzed using the OMNIC software.

(C) Illustration of the cyanine 3 and 6-fluorescein amidite fluorescent labels attached to the probe DNA and analyte DNA (SARS-CoV-2, SARS-CoV, and MERS-CoV DNA), respectively. The fluorescence spectra were measured at λ = 563 and 520 nm before and after DNA hybridization.

(D) Schematic showing the SARS-CoV-2 detection strategy using DNA hybridization between probe and analyte DNA. Direct fluorescence images of probe and analyte DNA. [Probe DNA] and [Analyte DNA] = 5 μM. The green fluorescence response depends on DNA hybridization when detecting the analyte DNA.

increasing with higher concentrations of APTES. Following probe DNA immobilization, it is observed to peak at 1,488, 1,645, 1,682, and 1,715 cm^{-1}, corresponding to the adenine,[48] thymine,[49] guanine,[50] and cytosine,[51] respectively. The ATR-FT-IR spectrum after hybridization with target DNA exhibits similar peaks with increased peak intensity. These results indicate successful immobilization of probe DNA and hybridization with target DNA.

For further validation of target DNA detection, we compared the fluorescence response using cyanine 3 (Cy3: red) and 6-fluorescein phosphoramidite (FAM: green) dye. Figure 3C illustrates the design strategy. The 3′-end of the probe DNA and the 5′-end of the target DNA and non-target (SAR-CoV and MERS-CoV) DNA are labeled with Cy3 and FAM, respectively. After the chemical reaction between APTES and probe DNA on the IGZO surface, probe DNA exhibits red fluorescence emission as a result of immobilization on the IGZO surface. Upon reaction of the target and non-target DNA, the Cy3 labeled probe DNA on the IGZO surface only hybridizes to target DNA to form a duplex DNA structure by hydrogen bond, resulting in the release of the strong green fluorescence emission as shown in Figure 3D. All results support the specific detection of target DNA by IGZO-EGTFTs.

Detection of SARS-CoV-2 DNA with sensitivity, selectivity, and recyclability

To evaluate the feasibility of SARS-CoV-2 DNA detection, the electrical analysis of a step-by-step process was conducted. Figure 4A shows the transfer characteristics of IGZO-EGTFTs according to each step modification, such as pristine IGZO, APTES treatment, probe DNA immobilization, and SARS-CoV-2 DNA hybridization in PBS. From the transfer characteristics, the V_{TH} value, which was determined for all 60 devices and plotted using the conventional linear extrapolation method in the linear region, shows a positive shift, as shown in Figure S6. First, the hydroxylation by oxygen plasma reduced the positive charge on the IGZO surface after the hydroxyl groups combined with the IGZO surface. When the APTES covalently bonded on the hydroxylated IGZO surface through the dehydration-condensation reaction, the drain current was

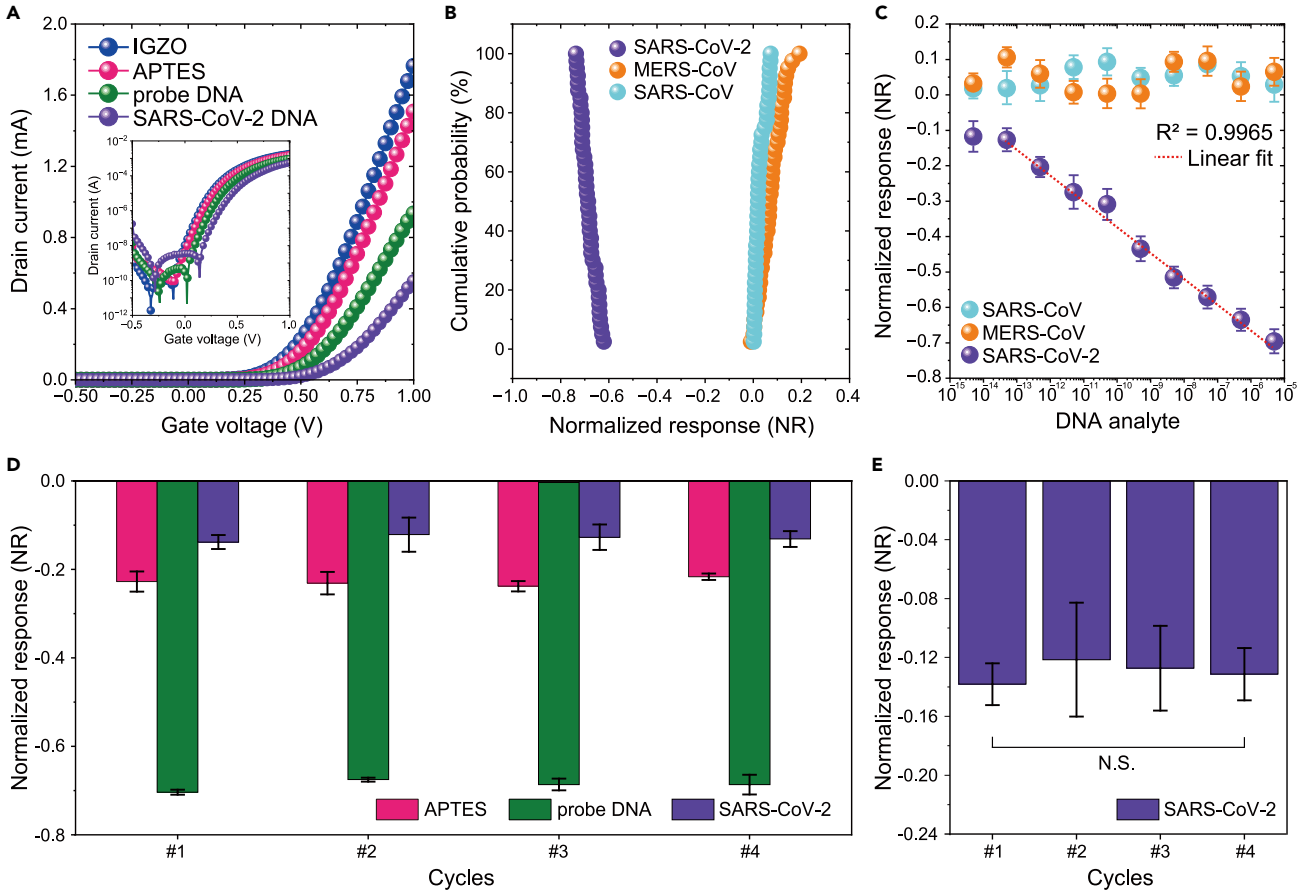

Figure 4. Electrical response of IGZO-EGTFT for detecting SARS-CoV-2 DNA

(A) Transfer characteristics of the IGZO-EGTFTs following APTES treatment, probe DNA immobilization, and SARS-CoV-2 DNA hybridization at a linear scale in PBS solution. The inset shows the transfer characteristics at the logarithmic scale in PBS solution.

(B) Selectivity responses of IGZO-EGTFTs toward SARS-CoV-2, SARS-CoV, and MERS-CoV DNA using cumulative probability distribution function (CDF) of NR for the entire ensemble of 135 devices. They confirm the excellent selectivity of the current response. Measurements are shown for the NR of the IGZO-EGTFTs extracted from the transfer curves.

(C) NR of IGZO-EGTFTs for different concentrations of SARS-CoV-2, SARS-CoV, and MERS-CoV DNA. The plot shows the wide detection range and linear response for SARS-CoV-2 DNA concentration from 5 fM to 5 μM. The detection limit was determined to be 50 fM. The error bars were calculated from three parallel experiments.

(D) Comparison of the NR after APTES treatment, probe DNA immobilization, and SARS-CoV-2 DNA hybridization at four cycles.

(E) Reversible and repeatable detection of SARS-CoV-2 DNA up to four cycles. N.S. indicates "non-significant".

gradually decreased by the APTES deposited on the IGZO surface. This trend is confirmed by different ATPES concentrations ranging from 1% to 15%, as shown in Figure S7. The initial stage of silanization (1% APTES), in which APTES molecules react with the abundant hydroxyl group on the IGZO surface, significantly increased the V_{TH} value. As the silanization reaction progressed and the decrease in the available reaction sites on the IGZO surface continued, the density of amine groups on the IGZO eventually saturated after reaching a sufficient concentration of APTES (10%).

Effective probe DNA immobilization is dependent on the quality of the functionalized APTES layer on IGZO surfaces. The concentration of APTES is a crucial parameter affecting the anchoring quality of probe DNA with high reliability. In the case of an excessively low APTES concentration, the resulting monolayer on the surface may be rendered incomplete and less stable, resulting in poor adhesion of the IGZO sensing layers or functional molecules.[52] Conversely, when an excessively high APTES concentration is used, the silane molecules may form multilayers or aggregates on the surface, which can also compromise the stability and homogeneity of the modification, as shown in Figure S8. The concentration of the probe DNA and the reaction time were found to be important factors affecting the hybridization of the SARS-CoV-2 DNA. As the concentration of the probe DNA increased, the measured normalized response (NR) decreased substantially and reached saturation at a concentration of 5 μM. Thus, it was concluded that a 10% of APTES concentration and 5 μM of probe DNA for surface modification of IGZO active layer was optimal for our biosensor, as this concentration resulted in a reduction in the NR from 0 to −0.712 (Figure S9). Additionally, the surface modification time for the DNA immobilization was also determined via the assessment of the

effects of varying modification times from 1 h to 4 h, as shown in Figure S10. An increase in the modification time from 1 to 3 h resulted in a significant change in NR due to immobilized probe DNA onto the APTES layer. By contrast, the extension beyond 3 h did not result in any significant change in NR. Consequently, a reaction time of 3 h was deemed optimal experimental condition for the probe DNA immobilization process.

By optimizing the experimental conditions, the IGZO surface was effectively functionalized for detecting SARS-CoV-2 DNA. Furthermore, based on the DNA sequence, the SARS-CoV-2 DNA could be used to hybridize with a probe DNA, resulting in the formation of a double-stranded DNA (dsDNA) molecule via hydrogen bonding between the base pairs (adenine with thymine and guanine with cytosine). However, the SARS-CoV and MERS-CoV DNA is incapable of hybridization because the sequence is not complementary to the probe DNA, thereby preventing the formation of a dsDNA molecule (Figure S11). The hybridization of SARS-CoV-2 DNA exerted a V_{TH} shift significantly toward the positive direction. These results were primarily caused by potential drops between the IGZO surface and electrolyte owing to the relatively large negative charge of the phosphate backbone of the DNA on the surface after the binding interaction. Thus, a larger positive gate voltage is required to turn the IGZO-EGTFTs when compared with that required for the pristine IGZO and APTES-deposited surfaces. Finally, to evaluate interference with various biomolecules, including growth factors, proteins, trace elements, vitamins, and hormones, transfer characteristics of IGZO-EGTFTs were investigated according to each step modification in FBS solution (Figure S12). The result confirmed that the presence of a diverse mix of biomolecules in FBS does not compromise the electrical performance of the IGZO-EGTFTs.

The cumulative probability of NR values was evaluated under the optimal experimental conditions to verify the selectivity for SARS-CoV-2 DNA. The results confirmed that SARS-CoV-2 DNA caused a statistically dramatic decrease in the NR values ($\Delta I/I_0 = -0.685$), whereas SARS-CoV and MERS-CoV DNA caused an invariant response in the saturation region, as shown in Figure 4B.

To determine the sensitivity of the IGZO-EGTFTs, several concentrations of SARS-CoV-2, SARS-CoV, and MERS-CoV DNA were evaluated using electrical analysis, as shown in Figure 4C. The results verified that IGZO-EGTFTs exhibited an excellent linear response to the SARS-CoV-2 DNA, with a high correlation coefficient (R^2) of 0.9965 and a wide detection range from 50 fM to 5 μM (limit of detection of 50 fM). Therefore, the IGZO-EGTFTs demonstrated good linearity in a wide detecting range and prominent sensitivity when compared to those of previously reported electrochemical DNA sensors (Table S4).

We also examined the time-dependent variation in the drain current of the IGZO-EGTFT, maintaining consistent S/D and gate voltages, as shown in Figure S13. Over time, the output values of the IGZO-EGTFT biosensor, functionalized with probe DNA for SARS-CoV-2 DNA detection, varied at a concentration of 5 μM. With the increase in reaction time between the probe DNA and SARS-CoV-2 DNA, there was a significant decrease in the measured normalized response, which eventually stabilized after reaching an optimal reaction time of 60 min.

Finally, we conducted a recyclable test to determine whether the device maintained its sensitivity following repeated use. The IGZO surface was cleaned via a simple oxygen plasma treatment, which removed the redundant biomolecules and reactivated the IGZO active layer, as shown in Figure S14. Figure 4D shows that the fabricated biosensor based on IGZO-EGTFTs maintained its sensitivity and linear response to the SARS-CoV-2 DNA even after four cycles of biofunctionalization and removal. Therefore, the IGZO-EGTFTs can be effectively reused without loss of their sensing capabilities, indicating excellent recyclability. This is a significant finding, as it renders the DNA sensor a cost-effective and sustainable option for diagnostic biosensing applications. Based on a one-way analysis of the variance test, it was determined that there were no statistically significant differences in the measured data of the NR values across the repeated cycles, with a p value greater than 0.05. In addition, the IGZO-EGTFTs maintained a consistent level of sensitivity, as evidenced by the NR values remaining at approximately −0.14, as shown in Figures 4E and S15. Therefore, the IGZO-EGTFTs could effectively detect SAS-CoV-2 DNA being measured while also being sufficiently robust to withstand repeated use. Overall, this is an indispensable characteristic for biosensors as it facilitates their reuse and reduces the waste associated with disposable sensors. The IGZO-EGTFTs maintained their sensitivity and reliability even after multiple uses, further supporting the excellent recyclability of the biosensor.

Conclusions

In this study, a SARS-CoV-2 DNA biosensor that exhibits unprecedented sensitivity and a comprehensive detection spectrum was demonstrated by IGZO-EGTFTs submerged in PBS solution with operational voltage under 1V, an environment that closely mimics physiological conditions. Through a rigorous, step-by-step process of molecular modification on the IGZO surface, we have augmented the probe DNA's binding capacity, which has been engineered to specifically recognize and latch onto SARS-CoV-2 DNA. This precise molecular interaction between the probe and target DNA has enabled a low detection limit of 50 fM and a broad-range detection capacity up to 5 μM with high selectivity. Moreover, the recyclability of the biosensor was demonstrated by the regeneration of the IGZO surface following a rapid and cost-effective cleaning process using oxygen plasma treatment, thus enabling its reuse in resource-limited environments. With these defining characteristics, this SARS-CoV-2 biosensor can play a pivotal role in the timely and effective detection of the virus, transforming our ability to monitor and respond to this global health crisis. Furthermore, this work can lay the foundation to explore future high-performance SARS-CoV-2 DNA biosensor based on IGZO-EGTFTs for achieving ultra-low detection limits. We believe the design principles elucidated in this study will be instrumental in guiding the development of next-generation biosensors for various biomedical applications.

Limitations of the study

In this study, we developed the significant advancements made in the field of nanoscale biofunctionalization at the solid-liquid interface. Our study focuses on detecting the SARS-CoV-2 DNA at low concentrations and ensuring that the detection is quantitative and reliable in the presence of a myriad of biomolecules. However, we did not detect SARS-CoV-2 DNA in clinical samples such as saliva and sputum nor a

comparison of these detection results with current PCR-based methods. Future studies are warranted to validate the results of this study in clinical samples and ensure quantitative and reliable detection of SARS-CoV-2.

STAR★METHODS

Detailed methods are provided in the online version of this paper and include the following:

- KEY RESOURCES TABLE
- RESOURCE AVAILABILITY
  - Lead contact
  - Materials availability
  - Data and code availability
- METHOD DETAILS
  - IGZO precursor preparation
  - Fabrication of IGZO-EGTFT biosensor
  - PDMS well preparation
  - Surface functionalization for DNA hybridization
  - Surface characterization
  - Detection of SARS-CoV-2
  - Recyclability test
  - Electrical characterization
- QUANTIFICATION AND STATISTICAL ANALYSIS

SUPPLEMENTAL INFORMATION

Supplemental information can be found online at https://doi.org/10.1016/j.isci.2024.109061.

ACKNOWLEDGMENTS

This research was supported by Basic Science Research Program through the National Research Foundation of Korea (NRF) funded by the Ministry of Education (RS-2023-00245734, RS-2023-00213089, and RS-2023-00220077). This research was supported by the MSIT (Ministry of Science and ICT), Korea, under the ITRC (Information Technology Research Center) support program (IITP-2023-2020-0-01461) supervised by the IITP (Institute for Information & communications Technology Planning & Evaluation). This work was supported by the Technology Innovation Program (Grant No. RS-2022-00154781) and Bio-convergence Technology Education Program (No. P0017805) funded by the Ministry of Trade, Industry & Energy (MOTIE, Korea). This research was also supported by Nano·Material Technology Development Program through the National Research Foundation of Korea (NRF) funded by the Ministry of Science, ICT and Future Planning (2009-0082580).

AUTHOR CONTRIBUTIONS

C.H.: Design of experiment, electrical characterization, methodology, data analysis, writing. S.B.: Electrical characterization, Y.S.: Electrical characterization, W.-J.L.: Data analysis and writing. S.P.: Project administration, writing-review and editing.

DECLARATION OF INTERESTS

The authors declare no competing interests.

Received: September 18, 2023
Revised: November 27, 2023
Accepted: January 25, 2024
Published: February 1, 2024

REFERENCES

1. Li, X., Zai, J., Wang, X., and Li, Y. (2020). Potential of large "first generation" human-to-human transmission of 2019-nCoV. J. Med. Virol. *92*, 448–454. https://doi.org/10.1002/jmv.25693.
2. Jiang, N., Tansukawat, N.D., Gonzalez-Macia, L., Ates, H.C., Dincer, C., Güder, F., Tasoglu, S., and Yetisen, A.K. (2021). Low-Cost Optical Assays for Point-of-Care Diagnosis in Resource-Limited Settings. ACS Sens. *6*, 2108–2124. https://doi.org/10.1021/acssensors.1c00669.
3. Li, C., Ji, F., Wang, L., Wang, L., Hao, J., Dai, M., Liu, Y., Pan, X., Fu, J., Li, L., et al. (2020). Asymptomatic and Human-to-Human Transmission of SARS-CoV-2 in a 2-Family Cluster, Xuzhou, China. Emerg. Infect. Dis. *26*, 1626–1628. https://doi.org/10.3201/eid2607.200718.
4. Fraiman, J., Erviti, J., Jones, M., Greenland, S., Whelan, P., Kaplan, R.M., and Doshi, P. (2022). Serious adverse events of special interest following mRNA COVID-19 vaccination in randomized trials in adults. Vaccine *40*, 5798–5805. https://doi.org/10.1016/j.vaccine.2022.08.036.
5. Richman, D.D. (2021). COVID-19 vaccines: implementation, limitations and opportunities. Glob. Health Med. *3*, 1–5. https://doi.org/10.35772/ghm.2021.01010.
6. Long, Q.-X., Tang, X.-J., Shi, Q.-L., Li, Q., Deng, H.-J., Yuan, J., Hu, J.-L., Xu, W., Zhang,

Y., Lv, F.-J., et al. (2020). Clinical and immunological assessment of asymptomatic SARS-CoV-2 infections. Nat. Med. *26*, 1200–1204. https://doi.org/10.1038/s41591-020-0965-6.

7. Skittrall, J.P., Wilson, M., Smielewska, A.A., Parmar, S., Fortune, M.D., Sparkes, D., Curran, M.D., Zhang, H., and Jalal, H. (2021). Specificity and positive predictive value of SARS-CoV-2 nucleic acid amplification testing in a low-prevalence setting. Clin. Microbiol. Infect. *27*, 469.e9–469.e15. https://doi.org/10.1016/j.cmi.2020.10.003.
8. Möckel, M., Corman, V.M., Stegemann, M.S., Hofmann, J., Stein, A., Jones, T.C., Gastmeier, P., Seybold, J., Offermann, R., Bachmann, U., et al. (2021). SARS-CoV-2 antigen rapid immunoassay for diagnosis of COVID-19 in the emergency department. Biomarkers. *26*, 213–220. https://doi.org/10.1080/1354750X.2021.1876769.
9. Clark, K.M., Schenkel, M.S., Pittman, T.W., Samper, I.C., Anderson, L.B.R., Khamcharoen, W., Elmegerhi, S., Perera, R., Siangproh, W., Kennan, A.J., et al. (2022). Electrochemical Capillary Driven Immunoassay for Detection of SARS-CoV-2. ACS Meas. Sci. Au *2*, 584–594. https://doi.org/10.1021/acsmeasuresciau.2c00037.
10. Ang, G.Y., Chan, K.G., Yean, C.Y., and Yu, C.Y. (2022). Lateral Flow Immunoassays for SARS-CoV-2. Diagnostics *12*, 2854. https://doi.org/10.3390/diagnostics12112854.
11. Leli, C., Di Matteo, L., Gotta, F., Cornaglia, E., Vay, D., Megna, I., Pensato, R.E., Boverio, R., and Rocchetti, A. (2021). Performance of a SARS-CoV-2 antigen rapid immunoassay in patients admitted to the emergency department. Int. J. Infect. Dis. *110*, 135–140. https://doi.org/10.1016/j.ijid.2021.07.043.
12. Rashed, M.Z., Kopechek, J.A., Priddy, M.C., Hamorsky, K.T., Palmer, K.E., Mittal, N., Valdez, J., Flynn, J., and Williams, S.J. (2021). Rapid detection of SARS-CoV-2 antibodies using electrochemical impedance-based detector. Biosens. Bioelectron. *171*, 112709. https://doi.org/10.1016/j.bios.2020.112709.
13. Zamzami, M.A., Rabbani, G., Ahmad, A., Basalah, A.A., Al-Sabban, W.H., Nate Ahn, S., and Choudhry, H. (2022). Carbon nanotube field-effect transistor (CNT-FET)-based biosensor for rapid detection of SARS-CoV-2 (COVID-19) surface spike protein S1. Bioelectrochemistry *143*, 107982. https://doi.org/10.1016/j.bioelechem.2021.107982.
14. Krüger, L.J., Gaeddert, M., Köppel, L., Brümmer, L.E., Gottschalk, C., Miranda, I.B., Schnitzler, P., Kräusslich, H.G., Lindner, A.K., Nikolai, O., et al. (2020). Evaluation of the Accuracy, Ease of Use and Limit of Detection of Novel, Rapid, Antigen-Detecting Point-Of-Care Diagnostics for *SARS-CoV-2* (Infectious Diseases (Except HIV/AIDS)). https://doi.org/10.1101/2020.10.01.20203836.
15. Liu, G., and Rusling, J.F. (2021). COVID-19 Antibody Tests and Their Limitations. ACS Sens. *6*, 593–612. https://doi.org/10.1021/acssensors.0c02621.
16. Wang, X., Wei, M., Li, X., Shao, S., Ren, Y., Xu, W., Li, M., Liu, W., Liu, X., and Zhao, J. (2020). Large-Area Flexible Printed Thin-Film Transistors with Semiconducting Single-Walled Carbon Nanotubes for NO_2 Sensors. ACS Appl. Mater. Interfaces *12*, 51797–51807. https://doi.org/10.1021/acsami.0c13824.
17. Kumar, N., Kumar, J., and Panda, S. (2016). Enhanced pH sensitivity over the Nernst limit of electrolyte gated a-IGZO thin film transistor using branched polyethylenimine. RSC Adv. *6*, 10810–10815. https://doi.org/10.1039/C5RA26409J.
18. Ma, P., Du, L., Wang, Y., Jiang, R., Xin, Q., Li, Y., and Song, A. (2018). Low voltage operation of IGZO thin film transistors enabled by ultrathin Al_2O_3 gate dielectric. Appl. Phys. Lett. *112*, 023501. https://doi.org/10.1063/1.5003662.
19. Wu, X., Surendran, A., Ko, J., Filonik, O., Herzig, E., Müller-Buschbaum, P., and Leong, W. (2018). Ionic-Liquid Doping Enables High Transconductance, Fast Response Time, and High Ion Sensitivity in Organic Electrochemical Transistors. Adv. Mater. *31*, 1805544. https://doi.org/10.1002/adma.201805544.
20. Park, S., Lee, S., Kim, C.-H., Lee, I., Lee, W.-J., Kim, S., Lee, B.-G., Jang, J.-H., and Yoon, M.-H. (2015). Sub-0.5 V Highly Stable Aqueous Salt Gated Metal Oxide Electronics. Sci. Rep. *5*, 13088. https://doi.org/10.1038/srep13088.
21. Liu, N., Chen, R., and Wan, Q. (2019). Recent Advances in Electric-Double-Layer Transistors for Bio-Chemical Sensing Applications. Sensors *19*, 3425. https://doi.org/10.3390/s19153425.
22. Woo Son, H., Park, J.H., Chae, M.-S., Kim, B.-H., and Kim, T.G. (2020). Bilayer indium gallium zinc oxide electrolyte-gated field-effect transistor for biosensor platform with high reliability. Sens. Actuators B Chem. *312*, 127955. https://doi.org/10.1016/j.snb.2020.127955.
23. Tappertzhofen, S. (2022). Impact of electrode materials on the performance of amorphous IGZO thin-film transistors. MRS Adv *7*, 723–728. https://doi.org/10.1557/s43580-022-00298-z.
24. Chae, M.-S., Park, J.H., Son, H.W., Hwang, K.S., and Kim, T.G. (2018). IGZO-based electrolyte-gated field-effect transistor for in situ biological sensing platform. Sens. Actuators B Chem. *262*, 876–883. https://doi.org/10.1016/j.snb.2018.02.090.
25. Hwang, C., Kwak, T., Kim, C.-H., Kim, J.H., and Park, S. (2022). Quantitative and rapid detection of iodide ion via electrolyte-gated IGZO thin-film transistors. Sens. Actuators B Chem. *353*, 131144. https://doi.org/10.1016/j.snb.2021.131144.
26. Kim, S., Lee, S.E., Park, J.H., Shin, J.Y., Lee, B., Lim, H.Y., Oh, Y.T., Hwang, J.P., Seon, S.W., Kim, S.H., et al. (2021). High Performance Field-Effect Transistors Based on Partially Suspended 2D Materials via Block Copolymer Lithography. Polymers *13*, 566. https://doi.org/10.3390/polym13040566.
27. Ionescu, A.M., and Riel, H. (2011). Tunnel field-effect transistors as energy-efficient electronic switches. Nature *479*, 329–337. https://doi.org/10.1038/nature10679.
28. Corman, V.M., Landt, O., Kaiser, M., Molenkamp, R., Meijer, A., Chu, D.K., Bleicker, T., Brünink, S., Schneider, J., Schmidt, M.L., et al. (2020). Detection of 2019 novel coronavirus (2019-nCoV) by real-time RT-PCR. Euro Surveill. *25*. https://doi.org/10.2807/1560-7917.ES.2020.25.3.2000045.
29. Kim, H., Park, M., Hwang, J., Kim, J.H., Chung, D.-R., Lee, K.S., and Kang, M. (2019). Development of Label-Free Colorimetric Assay for MERS-CoV Using Gold Nanoparticles. ACS Sens. *4*, 1306–1312. https://doi.org/10.1021/acssensors.9b00175.
30. Hwang, C., Park, N., Kim, E.S., Kim, M., Kim, S.D., Park, S., Kim, N.Y., and Kim, J.H. (2021). Ultra-fast and recyclable DNA biosensor for point-of-care detection of SARS-CoV-2 (COVID-19). Biosens. Bioelectron. *185*, 113177. https://doi.org/10.1016/j.bios.2021.113177.
31. Miranda, A., Martínez, L., and De Beule, P.A.A. (2020). Facile synthesis of an aminopropylsilane layer on Si/SiO2 substrates using ethanol as APTES solvent. MethodsX *7*, 100931. https://doi.org/10.1016/j.mex.2020.100931.
32. Mohamad Nor, N., Arivalakan, S., Zakaria, N.D., Nilamani, N., Lockman, Z., and Abdul Razak, K. (2022). Self-Assembled Iron Oxide Nanoparticle-Modified APTES-ITO Electrode for Simultaneous Stripping Analysis of Cd(II) and Pb(II) Ions. ACS Omega *7*, 3823–3833. https://doi.org/10.1021/acsomega.1c07158.
33. Yin, Z., He, Q., Huang, X., Zhang, J., Wu, S., Chen, P., Lu, G., Chen, P., Zhang, Q., Yan, Q., and Zhang, H. (2012). Real-time DNA detection using Pt nanoparticle-decorated reduced graphene oxide field-effect transistors. Nanoscale *4*, 293–297. https://doi.org/10.1039/C1NR11149C.
34. Vashist, S.K., Lam, E., Hrapovic, S., Male, K.B., and Luong, J.H.T. (2014). Immobilization of Antibodies and Enzymes on 3-Aminopropyltriethoxysilane-Functionalized Bioanalytical Platforms for Biosensors and Diagnostics. Chem. Rev. *114*, 11083–11130. https://doi.org/10.1021/cr5000943.
35. Kim, Y.G., Tak, Y.J., Kim, H.J., Kim, W.-G., Yoo, H., and Kim, H.J. (2018). Facile fabrication of wire-type indium gallium zinc oxide thin-film transistors applicable to ultrasensitive flexible sensors. Sci. Rep. *8*, 5546. https://doi.org/10.1038/s41598-018-23892-4.
36. Pavlov, V., Xiao, Y., Gill, R., Dishon, A., Kotler, M., and Willner, I. (2004). Amplified Chemiluminescence Surface Detection of DNA and Telomerase Activity Using Catalytic Nucleic Acid Labels. Anal. Chem. *76*, 2152–2156. https://doi.org/10.1021/ac035219l.
37. Gunnarsson, A., Jönsson, P., Marie, R., Tegenfeldt, J.O., and Höök, F. (2008). Single-Molecule Detection and Mismatch Discrimination of Unlabeled DNA Targets. Nano Lett. *8*, 183–188. https://doi.org/10.1021/nl072401j.
38. A Evtugyn, G., Hianik, T., and Hianik, T. (2011). Layer-by-Layer Polyelectrolyte Assembles Involving DNA as a Platform for DNA Sensors. Curr. Anal. Chem. *7*, 8–34. https://doi.org/10.2174/157341111793797626.
39. Walsh, M.K., Wang, X., and Weimer, B.C. (2001). Optimizing the immobilization of single-stranded DNA onto glass beads. J. Biochem. Biophys. Methods *47*, 221–231. https://doi.org/10.1016/S0165-022X(00)00146-9.
40. Qiu, L., Qiu, L., Wu, Z.-S., Shen, G., and Yu, R.-Q. (2013). Cooperative Amplification-Based Electrochemical Sensor for the Zeptomole Detection of. Nucleic Acids. Anal. Chem. *85*, 8225–8231. https://doi.org/10.1021/ac401300a.
41. Li, K., Tu, J., Zhang, Y., Jin, D., Li, T., Li, J., Ni, W., Xiao, M.-M., Zhang, Z.-Y., and Zhang, G.-J. (2022). Ultrasensitive detection of exosomal miRNA with PMO-graphene quantum dots-functionalized field-effect transistor biosensor. iScience *25*, 104522. https://doi.org/10.1016/j.isci.2022.104522.
42. Kong, D., Wang, X., Gu, C., Guo, M., Wang, Y., Ai, Z., Zhang, S., Chen, Y., Liu, W., Wu, Y., et al. (2021). Direct SARS-CoV-2 Nucleic Acid Detection by Y-Shaped DNA Dual-Probe Transistor Assay. J. Am. Chem. Soc. *143*,

17004–17014. https://doi.org/10.1021/jacs.1c06325.

43. Girifalco, L.A., and Good, R.J. (1957). A Theory for the Estimation of Surface and Interfacial Energies. I. Derivation and Application to Interfacial Tension. J. Phys. Chem. *61*, 904–909. https://doi.org/10.1021/j150553a013.
44. Zeng, X., Xu, G., Gao, Y., and An, Y. (2011). Surface Wettability of (3-Aminopropyl) triethoxysilane Self-Assembled Monolayers. J. Phys. Chem. B *115*, 450–454. https://doi.org/10.1021/jp109259b.
45. Chaudhary, S., Kamra, T., Uddin, K.M.A., Snezhkova, O., Jayawardena, H.S.N., Yan, M., Montelius, L., Schnadt, J., and Ye, L. (2014). Controlled short-linkage assembly of functional nano-objects. Appl. Surf. Sci. *300*, 22–28. https://doi.org/10.1016/j.apsusc.2014.01.174.
46. Wang, J., Wang, H., Wang, Y., Li, J., Su, Z., and Wei, G. (2014). Alternate layer-by-layer assembly of graphene oxide nanosheets and fibrinogen nanofibers on a silicon substrate for a biomimetic three-dimensional hydroxyapatite scaffold. J. Mater. Chem. B *2*, 7360–7368. https://doi.org/10.1039/C4TB01324G.
47. Gunda, N.S.K., Singh, M., Norman, L., Kaur, K., and Mitra, S.K. (2014). Optimization and characterization of biomolecule immobilization on silicon substrates using (3-aminopropyl)triethoxysilane (APTES) and glutaraldehyde linker. Appl. Surf. Sci. *305*, 522–530. https://doi.org/10.1016/j.apsusc.2014.03.130.
48. Tsuboi, M., Takahashi, S., and Harada, I. (1973). CHAPTER 11 - Infrared and Raman Spectra of Nucleic Acids—Vibrations in the Base-residues. In Structural Studies on Nucleic Acids and Other Biopolymers, J. Duchesne, ed. (Academic Press), pp. 91–145. https://doi.org/10.1016/B978-0-12-222902-2.50009-3.
49. Dagneaux, C., Liquier, J., and Taillandier, E. (1995). FTIR Study of a Nonclassical dT10*dA10-dT10 Intramolecular Triple Helix. Biochemistry *34*, 14815–14818. https://doi.org/10.1021/bi00045a023.
50. Tsuboi, M. (1970). Application of Infrared Spectroscopy to Structure Studies of Nucleic Acids. Appl. Spectrosc. Rev. *3*, 45–90. https://doi.org/10.1080/05704927008081687.
51. Zhizhina, G.P., and Oleinik, E.F. (1972). Infrared Spectroscopy of Nucleic Acids. Russ. Chem. Rev. *41*, 258. https://doi.org/10.1070/RC1972v041n03ABEH002043.
52. Wang, G., Kim, T.-W., and Lee, T. (2011). Electrical transport characteristics through molecular layers. J. Mater. Chem. *21*, 18117. https://doi.org/10.1039/c1jm12702k.

STAR★METHODS

KEY RESOURCES TABLE

REAGENT or RESOURCE	SOURCE	IDENTIFIER
Chemicals, peptides, and recombinant proteins		
Indium nitrate hydrate	Sigma Aldrich	CAS No. 207398-97-8
Gallium nitrate hydrate	Sigma Aldrich	CAS No. 69365-72-6
zinc acetate dehydrate	Sigma Aldrich	CAS No. 5970-45-6
3-aminopropyltriethoxysilane	Sigma Aldrich	CAS No. 919-30-2
Ag/AgCl (3.0 M KCl) reference electrode	CH Instruments	CAT No. CHI111
2-methoxyethanol	Sigma Aldrich	CAS No. 109-86-4
Polydimethylsiloxane	Dow Corning	N/A
Fetal bovine serum	Sigma Aldrich	MFCD00132239
Phosphate Buffered Saline	Samchun Chemical	MFCD00131855
PDMS monomer (Sylgard 184A)	Dow Corning Co., Ltd	N/A
Curing agent (Sylgard 184B)	Dow Corning Co., Ltd	N/A
Oligonucleotides		
5′-GCATCTCCTGATGAGGTTCCACCTG-3′	Bioneer	N/A
5′- CAGGTGGAACCTCATCAGGAGATGC-3′	Bioneer	N/A
5′- CCAGGTGGAACATCATCCGGTGATGC-3′	Bioneer	N/A
5′- TACGAGCCCACTACTCCCATTTCGTCAGCG-3′	Bioneer	N/A
Software and algorithms		
Image J	Open source	N/A
Origin 2023 software	https://www.originlab.com	N/A

RESOURCE AVAILABILITY

Lead contact

Further information and requests for resources and reagents should be directed to and will be fulfilled by the lead contact, Sungjun Park (sj0223park@ajou.ac.kr).

Materials availability

No new reagents were developed in this study.

Data and code availability

- Date: Data reported in this paper will be shared by the lead contact upon request.
- Code: This paper does not report original code.
- All other requests: Any additional information required to reanalyze the data reported will be shared by the lead contact upon request.

METHOD DETAILS

IGZO precursor preparation

The IGZO precursor solution was prepared by dissolving In $(NO_3)_3 \cdot xH_2O$, Ga $(NO_3)_3 \cdot xH_2O$, and Zn $(CH_3COO)_2 \cdot 2H_2O$ in 2-methoxyethanol with a total concentration of 0.1 M at a molar ratio of In-Ga-Zn = 0.1:0.15:0.0275. The mixture was stirred at 60°C for 4 h, and the resulting precursor solution was filtered through a 0.2 μm hydrophobic polytetrafluoroethylene membrane-based syringe filter before deposition.

Fabrication of IGZO-EGTFT biosensor

To fabricate the samples, the substrates were prepared by thermal oxidation of a 300-nm-thick-layer of silicon dioxide on heavily boron-doped Si wafers. The source and drain electrodes were then fabricated using a combination of 10 nm titanium and 50 nm gold metals via e-beam evaporation and photolithography. Prior to spin coating the IGZO precursor solution onto the Si wafers, oxygen plasma treatment

was performed at a power of 100 W for 10 min to transform the hydrophobic surface of the Si wafers into a hydrophilic surface. Thereafter, the IGZO solution was spin coated at 4000 rpm for 30 s, followed by annealing the coated layers in air at 400°C for 1.5 h to form a densified metal-oxide-semiconductor layer. Consequently, the IGZO thin film was patterned via photolithography and wet etching processes.

PDMS well preparation

To prevent device degradation and ensure appropriate storage of the analyte solutions, the epoxy-based SU-8 3008 was deposited onto the device except at the active site. To form the PDMS well, two components—the base solution (Sylgard 184A) and curing agent (Sylgard 184B)—were mixed at a 10:1 ratio by weight and dried in a vacuum oven at 60°C for 4 h. Following the vacuum-thermal curing, the PDMS well was fabricated using 8 mm diameter punch holes attached to the top of the IGZO-EGTFTs. Accordingly, a sensing area of 50.24 mm^2 was obtained.

Surface functionalization for DNA hybridization

In the biofunctionalization process, the IGZO surface was initially modified to introduce hydroxyl groups by oxygen plasma treatment at a power of 60 W for 1 min. The treatment generated hydroxyl groups on the surface, which transformed its hydrophobicity to hydrophilicity. Subsequently, a solution of APTES was prepared by dissolving it in ethanol at a volumetric concentration of 10%. The APTES solution was then mixed using a vortex mixer for 3 min to disperse the APTES molecules in the solvent. Thereafter, the device was submerged in the solution for 17 h, which was followed by rinsing with DI water and blow drying with nitrogen to remove the weak bonds. The IGZO surface was modified with the amino functional group (-NH_2). The modification facilitated the covalent bonding of the probe DNA to the IGZO surface. In the second step of the biofunctionalization process, the APTES–probe DNA interaction was employed, wherein the APTES and probe DNA served as models for the crosslinking and receptor molecules, respectively. To immobilize the probe DNA to the modified IGZO surface, a DNA solution was prepared in DI water at a concentration of 5 μM and mixed using a vortex mixer for 2 min until complete dissolution. Thereafter, 20 μL of the DNA solution was applied to the surface and incubated at 60°C for 3 h. Following that, any unbound probe DNA was removed by washing the surface with DI water and drying it using nitrogen gas. The resulting devices were then stored for future use.

Surface characterization

Water contact angle (WCA) measurements were performed to estimate the surface free energies onto the pristine IGZO, APTES treatment, probe DNA immobilization, and target DNA hybridization. The analysis was conducted by dispensing DI water onto various chemical surfaces, followed by capturing a side-view photograph of the contact angle measurement using a digital camera (Phoenix-MT), which was then processed using image analysis software (Surfaceware 9). Fourier transform infrared spectroscopy (FT-IR) (NICOLET iS50, Thermo Fisher Scientific) was utilized to investigate APTES and DNA anchored to the IGZO surface. Furthermore, the probe DNA immobilization and the target DNA hybridization were validated by examining the IGZO surface using a fluorescence microscope (EVOS M7000, Thermo Fisher Scientific) and hybrid multimode reader (Synergy *Neo2*, Biotek).

Detection of SARS-CoV-2

Following the surface functionalization step, the probe DNA was utilized to prepare the biosensor as a receptor to detect the SARS-CoV-2 DNA. To obtain a 5 μM solution, both the complementary DNA (SARS-CoV-2) and non-complementary DNA (SARS-CoV and MERS-CoV) were dissolved in DI water and then diluted in PBS and FBS. To detect the target DNA in the hybridization reaction, 20 μL of this solution was placed onto the surface of the biosensor and allowed to incubate at 95°C for 5 min, followed by an additional incubation at room temperature for 1 h. This was done to reduce the likelihood of non-specific reactions occurring. Subsequently, the surface of the biosensor was rinsed three times with PBS and then blow-dried using nitrogen.

Recyclability test

To evaluate the recyclability of the biosensor, the modification in the drain current following the APTES treatment, probe DNA immobilization, and SARS-CoV-2 hybridization were measured each time the biosensor was reused. This sequence was repeated four times, and the variation in the drain current was assessed after each cycle.

Electrical characterization

The electrical characteristics of the IGZO-EGTFTs were measured after submerging an Ag/AgCl reference electrode (RE) containing a 1 M KCl internal filling solution in an electrolyte solution. To prevent parasitic leakage current, the source and drain electrodes were covered with an IGZO semiconductor. All reported potentials were biased with respect to a commercial Ag/AgCl RE (CHI111, CH Instruments). Additionally, a PDMS well was integrated with the IGZO-EGTFT to form a container for the electrical measurement. Subsequently, the Ag/AgCl RE was inserted into the PDMS well to stabilize the potential. The *I–V* characteristics were measured for all the fabricated IGZO-EGTFTs by using a Keithley 2602B dual-channel source meter with a sweep rate of 1000 mV/s under ambient conditions. Measurements were performed after each experimental step, including the APTES treatment, probe DNA immobilization, and SARS-CoV-2 DNA hybridization. The normalized response (NR) of the biosensor was calculated according to Equation 1.

$$\text{Normalized response (NR)} = \frac{|I_D - I_0|}{I_0} \quad \text{(Equation 1)}$$

where I_O and I_D are the drain current of the IGZO-EGTFT before and after reactions such as ATPES treatment, probe DNA immobilization, and target DNA hybridization, respectively.

QUANTIFICATION AND STATISTICAL ANALYSIS

We used Microsoft 365 Excel software (Microsoft Corp.; Redmond, WA, USA) to record the individual results and calculate the statistical significance. For the case when the p value was less than 0.05, a significant difference was considered between the two experimental values. All graphs were plotted using the OriginPro 2023 software (OriginLab Corporation, Northampton, MA, USA).